

This is a pre print version of the following article:

GAPses: Versatile smart glasses for comfortable and fully-dry acquisition and parallel ultra-low-power processing of EEG and EOG / Frey, S.; Lucchini, M. A.; Kartsch, V.; Ingolfsson, T. M.; Bernardi, A. H.; Segessenmann, M.; Osieleniec, J.; Benatti, S.; Benini, L.; Cossettini, A.. - In: IEEE TRANSACTIONS ON BIOMEDICAL CIRCUITS AND SYSTEMS. - ISSN 1932-4545. - 19:3(2025), pp. 616-628.  
[10.1109/TBCAS.2024.3478798]

*Terms of use:*

The terms and conditions for the reuse of this version of the manuscript are specified in the publishing policy. For all terms of use and more information see the publisher's website.

06/05/2026 00:59

(Article begins on next page)

# GAPses: Versatile smart glasses for comfortable and fully-dry acquisition and parallel ultra-low-power processing of EEG and EOG

Sebastian Frey, *Graduate Student Member, IEEE*, Mattia Alberto Lucchini, Victor Kartsch, *Member, IEEE*, Thorir Mar Ingólfsson, *Graduate Student Member, IEEE*, Andrea Helga Bernardi, Michael Segessenmann, Jakub Osieleniec, Simone Benatti, *Member, IEEE*, Luca Benini, *Fellow, IEEE*, and Andrea Cossettini, *Member, IEEE*

**Abstract**—Recent advancements in head-mounted wearable technology are revolutionizing the field of biopotential measurement, but the integration of these technologies into practical, user-friendly devices remains challenging due to issues with design intrusiveness, comfort, reliability, and data privacy. To address these challenges, this paper presents GAPSES, a novel smart glasses platform designed for unobtrusive, comfortable, and secure acquisition and processing of electroencephalography (EEG) and electrooculography (EOG) signals. We introduce a direct electrode-electronics interface within a sleek frame design, with custom fully dry soft electrodes to enhance comfort for long wear. The fully assembled glasses, including electronics, weigh 40 g and have a compact size of 160 mm x 145 mm. An integrated parallel ultra-low-power RISC-V processor (GAP9, Greenwaves Technologies) processes data at the edge, thereby eliminating the need for continuous data streaming through a wireless link, enhancing privacy, and increasing system reliability in adverse channel conditions. We demonstrate the broad applicability of the designed prototype through validation in a number of EEG-based interaction tasks, including alpha waves, steady-state visual evoked potential analysis, and motor movement classification. Furthermore, we demonstrate an EEG-based biometric subject recognition task, where we reach a sensitivity and specificity of 98.87% and 99.86% respectively, with only 8 EEG channels and an energy consumption per inference on the edge as low as 121  $\mu$ J. Moreover, in an EOG-based eye movement classification task, we reach an accuracy of 96.68% on 11 classes, resulting in an information transfer rate of 94.78 bit/min, which can be further increased to 161.43 bit/min by reducing the accuracy to 81.43%. The deployed implementation has an energy consumption of 24  $\mu$ J per inference and a total system power of only 16.28 mW, allowing for continuous operation of more than 12 h with a small 75 mAh battery.

**Index Terms**—BCI, EEG, embedded deployment, EOG, HMI, smart glasses, wearable devices

## I. INTRODUCTION

Biopotential measurement is currently undergoing a paradigm shift towards wearable technology, impacting the way we monitor our physiological functions and interact with our surroundings by enabling continuous, long-term monitoring [1]. Continuous monitoring has the potential to deepen our understanding of human physiological responses in various contexts, advancing assistive technologies and human-machine interaction beyond research laboratory settings [2].

This project was supported by the Swiss National Science Foundation (Project PEDESITE) under grant agreement 193813, by the ETH-Domain Joint Initiative program (project UrbanTwin), and by the ETH Future Computing Laboratory (EFCL).

Sebastian Frey, Victor Kartsch, Thorir Mar Ingólfsson, Luca Benini, and Andrea Cossettini are with the Integrated Systems Laboratory, ETH Zürich, Zürich, Switzerland.

Luca Benini is also with the DEI, University of Bologna, Bologna, Italy. Andrea Helga Bernardi is with the DEI, University of Bologna, Bologna, Italy.

Simone Benatti is with the DISMI, University of Modena and Reggio Emilia, Reggio Emilia, Italy, and with the DEI, University of Bologna, Bologna, Italy.

Mattia Lucchini, Michael Segessenmann, Jakub Osieleniec are with Dätwyler Schweiz AG, Schattdorf, Switzerland.

Various body locations are suitable for measuring biosignals, but the human head offers unparalleled opportunities for monitoring health, drowsiness, and cognitive states, thanks to the proximity to the brain and multiple sensory organs (e.g., the eyes, nose, and ears) [3]. For example, head-mounted wearables such as the cEEGrid [4] or the Emotiv Insight and EPOC+ [5] demonstrated advanced capabilities in neural signals monitoring, offering insights into brain activity for cognitive studies, mental health monitoring, and Brain-Computer Interfaces (BCIs) [6].

However, current research on wearable biopotential measurement devices faces significant challenges that impede widespread user acceptance and practical usage in unconstrained settings. The main limitations of existing head-mounted biopotential measurement systems include: (1) user acceptance hindered by obtrusive designs and unconventional aesthetics of the devices [7]; (2) achieving wearability and comfort remains difficult without the development of custom, soft electrodes that can conform to the individual's body without causing irritation or discomfort [8]; (3) streaming ExG data through low-power wireless links presents privacy concerns (sensitive information could potentially be intercepted or misused) as well as limited reliability and throughput (which can compromise the integrity and usefulness of the transmitted data, especially in real-time applications) [9], [10].

This work presents GAPSES, versatile smart glasses for inconspicuous, fully dry and wearable electroencephalography (EEG) and electrooculography (EOG) acquisition and onboard processing. To address the above challenges, GAPSES (1) feature a novel approach of direct electrode-electronics interfacing, resulting in an unobtrusive design that is lightweight and sleek, comparable to commodity passive glasses; (2) incorporate novel custom soft EEG and EOG electrodes that are designed for comfortable, fully dry acquisition of biopotentials over multiple hours of use; (3) integrate a Parallel Ultra Low Power (PULP) RISC-V processor that enables on-edge processing of biopotential data, thereby eliminating the need for continuous data streaming. Thanks to PULP onboard processing, GAPSES not only address substantial privacy concerns by reducing the risk of data interception, but also overcome issues related to bandwidth, reliability, and responsiveness of wireless connections (ensuring that the integrity and usefulness of the data are maintained, which is particularly crucial for applications requiring real-time processing). We showcase the platform's broad applicability in measuring high-quality EEG and EOG data across a range of commonly used EEG and EOG paradigms. In particular, we validate GAPSES in EOG-based eye movement tasks achieving high information transfer rate (ITR) and in EEG-based biometric identification, demonstrating their capabilities for end-to-end biopotential acquisition and edge processing at State-of-the-Art (SoA) energy efficiency.

The main contributions are the following:

- Design of a novel smart glasses platform (GAPSES) for unobtrusive, comfortable, and secure acquisition and processing of EEG and EOG signals. Custom, fully-dry soft electrodes are coupled with a direct electrode-electronics interface and a sleek

glasses frame design. The glasses weigh only 40 g and have a compact size of 160 mm x 145 mm.

- First-time integration of a highly versatile parallel ultra-low-power RISC-V platform in glasses form factor for biopotentials.
- Demonstration of the application of GAPSES on different use-cases for EOG and EEG, namely, EOG-based eye movement classification, standard EEG tasks (alpha waves, SSVEP, motor movement), and EEG-based biometrics. GAPSES achieve an eye movement classification accuracy of 96.68 % on 11 classes, with an ITR as high as 161.43 bit/min if when an accuracy of 81.43 % is considered sufficient. The EEG-based biometrics reach a sensitivity and specificity of 98.87 % and 99.86 % respectively.
- Deployment of the proposed classification tasks on the RISC-V-based edge device, achieving an energy consumption as low as 24  $\mu$ J per inference on the EOG classification task, coupled with an average power consumption of only 16.28 mW, thereby enabling continuous operation for more than 12 h with a small 75 mAh battery.

The paper is organized as follows. Section II discusses related work of wearable biopotential platforms and smart glasses, with a focus on EEG and EOG measurements. Section III presents the design of GAPSES with its main components: custom electrodes, frame, and acquisition and processing electronics. Section IV validates GAPSES with several common EEG paradigms (alpha waves, Steady State Visually Evoked Potential (SSVEP), and Motor Movement (MM)) and ocular movements (visual inspection of EOG signals). In section V, we showcase the application of GAPSES for an EOG-based task, namely, eye movement classification. In section VI, we showcase the application of GAPSES for EEG-based biometrics. Discussion and conclusion in Sect. VII-VIII conclude the paper.

## II. RELATED WORKS

### A. Biopotential data acquisition platforms

Examples of commercially available wireless EEG systems include the Emotiv Insight and EPOC+ [5], Neurosky MindWave [11], and OpenBCI cEEGrid and Ultracortex [4]. Of those, the Emotiv EPOC+ and OpenBCI cEEGrid are often used in research. The EMOTIV EPOC+ is designed as a headset featuring 14 EEG channels with a 14 bit resolution and streams the measured data at up to 256 SPS to a PC or mobile phone. The headset can be set up quickly but does not allow for the adaptation of the channel placement and relies on a constant wireless connection to another device. OpenBCI cEEGrid stands out with its open-source approach that allows for customization in terms of the form factor (e.g., headsets or around-the-ear solutions) and electrode positions and materials. It integrates the ADS1299, a widely used analog frontend (AFE) for biopotential measurements that allows to measure up to 8 EEG channels with a resolution of 24 bit at 256 SPS and the RFD22301 for a wireless Bluetooth Low Energy (BLE) connection.

Beyond commercial devices, several custom biopotential measurement platforms have been proposed in research. The work in [12] presents a headband and uses it for a depression detection task. The headband integrates three channel electrodes at the frontal lobe (Fp1, Fpz, Fp2) with bias and reference on the mastoids, and a custom PCB based on the ADS1299 for EEG measurement is located in a box and attached to the rear side of the headband. Using a similar approach of integrating a dedicated AFE for biopotential measurements, the work in [13] integrates the RHD2216 from Intan technologies (featuring a 16 bit Analog to Digital Converter (ADC)). The custom design makes use of a single EEG channel with the electrodes placed on

the forehead and on the right mastoid, and streams out the measured data via BLE (Bot-NLE522, CHIPSEN).

A major limitation of these devices is that they lack onboard computational capabilities and need to stream raw EEG data (possibly filtered) to a benchtop computer for processing, thereby facing the limitation of the bandwidth of the low-power data links [14]. In this work, we make use of BioGAP [15], a SoA biosignal acquisition and processing platform that features an ADS1298 AFE from Texas Instruments for analog-to-digital conversion of 8 ExG channels with 24 bit resolution and the possibility to interface both active and passive electrodes, allowing the customization of the electrode interfacing based on specific experimental needs. A key feature of BioGAP is its onboard processing capabilities powered by the GAP9 processor (GreenWaves Technologies). This enables the execution of complex digital signal processing (DSP) tasks and Machine Learning (ML) model inference directly on the device. By processing data on the edge, BioGAP effectively addresses the typical bandwidth limitations and reliability concerns associated with wireless data transmission, at the same time enhancing battery lifetime.

### B. Smart glasses for EEG and EOG sensing

A notable example of ExG glasses research prototype is e-Glass [16], equipped with four dry EEG electrodes embedded in the glasses frame for real-time epileptic seizure detection. The hardware includes a commercially available AFE (ADS1299, Texas Instruments) and a low-power microcontroller (STM32L151, STMicroelectronics) with limited onboard processing capabilities and wireless communication (nRF8001, Nordic Semiconductor). The authors evaluate the system's capabilities on a public dataset for seizure detection. The proposed algorithm is based on feature extraction using discrete wavelet transform (DWT) and the power in common EEG bands with subsequent classification using a random forest classifier. Classification is based on a subset of the channels available in the dataset, corresponding to the electrode positions in e-Glass. An embedded implementation of the proposed algorithm enables 2.71 days of operation with a 570 mAh battery.

The AttentivU platform [17], on the other hand, integrates into a pair of glasses both EEG and EOG sensors. The device is tailored for real-time monitoring of physiological signals for attention and engagement feedback and employs dry silver electrodes: two for EEG (TP9 and TP10), with the reference placed in the nose bridge, and two for EOG placed in the nose pads of the glasses. The system architecture consists of preprocessing blocks for EEG and EOG for analog filtering and amplification, followed by a 12 MHz microcontroller with an integrated 10 bit ADC. The glasses were validated by comparison with wet Ag/AgCl electrodes, and visual inspection of the signal in an alpha waves (AW) experiment (eyes open vs. eyes closed) for the EEG subsystem, and execution of eye movements for the EOG subsystem. The system can operate for 5 hours using a 150 mAh battery.

Another example of heterogeneous EOG-EEG sensing platform is the work in [18], presenting a study on 3D-printed smart glasses designed for wearable healthcare and human-machine interfaces (HMIs). The smart glasses integrate electrodes based on carbon nanotube/polydimethylsiloxane composites and feature UV-responsive, color-tunable lenses for dual eyeglass and sunglass functionality. They are capable of both EEG and EOG sensing and integrate accelerometers for tracking of human posture and behavior. The system features an ATmega128 microprocessor (Atmel Corp.) and Bluetooth connectivity, and consumes approximately 300 mWh.

Additional examples of commercial-grade systems include both EEG-based sensing platforms (Smith Lowdown Focus Eyewear

Glasses [19]) and EOG-based sensing platforms (JINS MEME [20], Imec Glasses [21]). Smith Lowdown Focus Eyewear features a lightweight design with dry EEG electrodes located at TP9 and TP10, aligning with the 10–20 EEG system. JINS MEME integrates three-point EOG sensors on the nose pads and bridge of the glasses frame, alongside an accelerometer and a gyroscope. The Imec Glasses follow a similar electrode placement but with two additional electrodes, one on each temple of the glasses. These systems aim to monitor and enhance cognitive performance. However, they require pairing with an external device, such as a smartphone, for operation. In addition, they are limited to a single modality and cannot run custom applications directly on the glasses.

However, while the above platforms offer promising functionalities, they operate on a single biosignal modality (EEG or EOG), feature a very small number of channels, or lack sufficient onboard processing capabilities to execute more advanced ML models on the edge. GAPSES overcome all these limitations, as presented in the following sections and shown in the SoA comparison table (Table V, further discussed later).

### III. SYSTEM DESIGN

Figure 1 shows the GAPSES smart glasses, which integrate: a frame (to support the entire system mechanically), the electrodes (custom dry design by Datwyler to capture EOG and EEG signals), an electrodes interface printed circuit board (PCB) (routing the signals from the electrodes to the acquisition device with signal buffering), a channel-selection interface PCB (allowing to select a subset of 8 channels, enabling either a full EEG or a combined EEG–EOG configuration), and BioGAP (signal acquisition and processing platform). In the following we describe each component in detail.

#### A. Electrodes: placement and design

The electrodes used in this work are a custom design based on the SoftPulse® technology by Datwyler [22]. SoftPulse® dry electrodes have been selected for this work as they allow collection of bio-signal without need of gel nor skin preparation, they are comfortable to wear for all-day use, and they allow easy customization of the design. Thanks to Datwyler’s customization capabilities, the electrodes can be designed according to customer requirements via an injection-molding approach (in-house tool design, mold shop, and production area give high flexibility and quality). The base material is a highly conductive rubber, which can also be combined with other materials like metal or thermoplasts. In this work, electrodes are made of a highly electrically conductive elastomer and feature a silver–silver chloride-based coating. Other electrode designs tailored for capturing physiological signals have already been presented previously [23], [24] and are commercially available [23].

All electrodes have been tested by an independent laboratory to meet the standards of biocompatibility (according to ISO 10993-5 [25], and ISO 10993-10 [26]).

In terms of performance, SoftPulse® electrodes have an electrode tissue impedance (ETI) of ca.  $5 \times 10^7 \Omega \text{ mm}^2$ , comparable to the one of metal electrodes and sintered Ag/AgCl electrodes.

For GAPSES, two types of electrodes have been custom-designed to fit within the available space of a regular glasses frame, while still maximizing the contact area with the skin to decrease the electrode-tissue impedance. Figure 1 (B) shows the two electrode types, which are tailored for the acquisition of EOG and EEG signals, respectively.

1) *EOG electrodes*: EOG signals are collected through three custom electrodes in the nose region. Two electrodes are placed on the nose pad, while a third one is fixed at the level of the nasion in the glass bridge (see Fig. 1, A). Since the body region in contact with

the EOG electrodes is not hairy, EOG electrodes have been designed with a flat surface to maximize skin contact area and minimize electrode-skin impedance. Considering the constraints coming from the glass frame, a surface area of ca.  $25 \text{ mm}^2$  for each electrode was considered.

2) *EEG electrodes*: EEG signals are collected using electrodes located in the back part of the glasses’ arms. Specifically, GAPSES feature three EEG channels on the temple and one channel Behind-the-Ear (BTE), on each side (see Fig. 1, A). Reference and bias are positioned on the temple tips at positions TP9 and TP10, respectively, according to the 10-20 reference system. Both reference and bias are obtained by connecting together two EEG electrodes, in order to maximize the contact area and stability. As the region around the ear might be hairy, EEG electrodes have been designed with prongs facing the users’ skin. The presence of legs on the electrodes’ surface allows contact with the skin without the need for shaving or additional skin preparation. The legs, their number, position, and orientation have been designed to allow maximum hair penetration, highest skin contact, and best comfort. In particular, the electrodes’ legs have been arranged in two rows shifted by  $45^\circ$ . This configuration has been specifically developed thinking on how eye glasses are worn by the user, from top-front to low-back. By adopting this angle, we expect the legs to have a more efficient brush effect between the hairs, therefore achieving better hair penetration. Legs’ height has also been designed specifically for integration in eyewear, with the final height of 2 mm being a compromise between effective hair penetration and user comfort. Each EEG electrode has an area of ca.  $12 \text{ mm}^2$  in contact with the skin.

#### B. Electrodes-frames interface

The connection between the electrodes and the electronics can be achieved by simple physical contact between the electrically conductive rubber body and the electronics. SoftPulse® electrodes are designed with a standard male ECG snap, and the connection is normally done by means of standard snap connectors. This configuration allows a firm and stable electrical connection, with the possibility of replacing the electrodes if needed. In this work, the use of a standard snap connector was not possible due to space limitations. In order to keep the possibility of exchanging electrodes in case of need while saving space at the same time, an ad-hoc snap mechanism has been developed. In particular, the male snap in the back of the electrodes (see Fig. 1, B) has been designed together with the rigid part of the electrode-interface PCB (Fig. 1, C) where a plated through hole (PTH) was envisioned. Thanks to the tight tolerances, the male snap can fit the PTH tightly in the PCB, and the metal contact allows the electrical connection.

#### C. Glasses frame

The design of the frame (Fig. 1, A) has been developed to fulfill both aesthetic and functional requirements. For this reason, the design is light and thin, similar to commonly available glass frames on the market. The frame is designed in the full-rim style that completely encircles the lenses, with temple tips slightly curved behind the ears for a secure fit.

The whole frame is made of three parts, namely the front part, the right temple arm, and the left temple arm. All parts have been 3D printed with SLA technology using a semi-rigid photopolymer resin. All parts have been designed as two separated sub-parts (facing inwards and outwards, respectively, with respect to the wearer’s perspective), empty inside to allow the incorporation of the electrodes interface PCB (see below), and are assembled with screws and nuts. The front frame has three apertures in the nose pad and bridge region

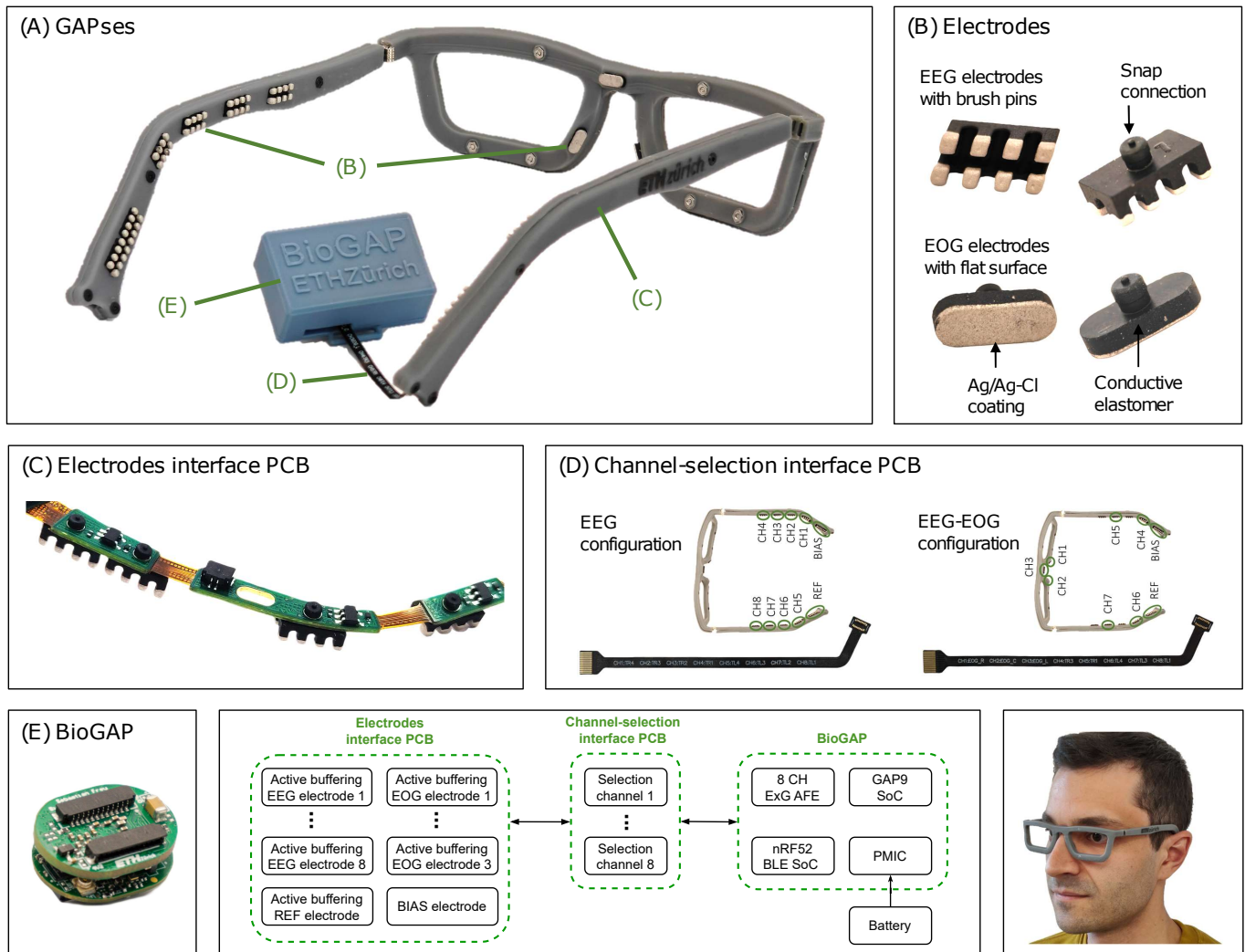


**Fig. 1.** (A) Photo of the whole system. (B) Detailed view of the custom EOG (flat) and EEG (brush) electrodes. (C) Electrode interface PCB, embedded in the glasses' frame. (D) Channel-selection interface PCB, used to select which channels (among the 3 EOG and 8 EEG channels available) are interfaced to BioGAP. Two alternative versions are designed, resulting in an EEG-only configuration or hybrid EEG+EOG configuration. (E) BioGAP acquisition and processing platform. The bottom block diagram shows the connectivity between the different PCBs and their internal key components. Bottom right: photo of a subject wearing GAPsEs

to allow the insertion of the EOG electrodes. Both temple arms have six openings to fix the EEG channel electrodes and the reference / bias electrodes (three EEG electrodes on the temples, one EEG electrode BTE electrode, two EEG electrodes connected together on the mastoids).

#### D. Electrodes interface PCB

Signals from the electrodes are routed to the acquisition device through a flex-rigid electrode-interface PCB (shown in Fig. 1, C). The flexible sections, integrated directly with rigid sections during manufacturing (eliminating the need for additional connectors), comprise two-layer, 0.11 mm-thick PCBs (ENIG finish) and are employed in areas prone to bending, such as the glass legs hinges and in between the electrodes. The rigid sections, comprising four-layer, 0.6 mm-thick PCBs, provide a mechanical attachment and electric contact to the electrodes via PTH with a diameter to pressure fit the snap extensions on the electrodes, allowing to attach electrodes without the need for a snap connector and hence, reducing the overall volume of the device. Rigid sections also incorporate a buffering subsystem (one per channel), based on the AD8603 (Analog Devices), used to reduce

signal interference and artifacts caused by movement while also enhancing the common-mode rejection ratio (CMRR). Each buffering subsystem is equipped with 68 k $\Omega$  protection resistors to limit the current to the subject in case of a fault. Electrodes in this design rely on a single-ended configuration (monopolar montage), hence, besides individual channel leads/electrodes, the device also incorporates a reference lead/electrode and a bias lead/electrode (more details in the next section). The electrodes interface PCB features eight EEG channels (three temple and one BTE channel on each side) and three EOG channels.

#### E. BioGAP data acquisition platform and channel selection interface

Data acquisition, processing, and wireless transmission are based on BioGAP [15] (Fig. 1, E). BioGAP is a wearable and compact bio-signal acquisition and processing platform that is compact ( $16 \times 21 \times 14 \text{ mm}^3$ ) and lightweight (6 g). BioGAP encompasses two stacked PCBs: a *baseboard* and a *bio-potential expansion board* that handles 8 ExG channels. BioGAP is connected to the glasses frame via a *channel-selection interface PCB* (Fig. 1, D) that selects which subset

of 8 channels from the electrodes-interface PCB (out of the 3 EOG + 8 EEG channels available) is to be acquired and processed.

1) *Baseboard*: The baseboard functions as the central unit for measurement control, signal processing, data handling, and power management. It hosts two System on Chips (SoCs): the nRF52811 from Nordic Semiconductor, which provides BLE connectivity, and the GAP9 parallel ultra-low-power (ULP) processor by GreenWaves Technologies, tailored for DSP computation and neural network (NN) inference with high energy efficiency [27]. The GAP9 processor delivers up to 15.6 GOP/s of DSP computational capability and 32.2 GMAC/s for ML tasks. It features automatic clock gating, voltage scaling, and adaptable and dynamic frequency scaling to optimize computational resources, minimize energy use, and facilitate extended device operation. The baseboard also incorporates 256 Mbit of volatile memory (APS256 series, APMemory) and 128 Mbit of non-volatile memory (MX25UW series, Macronix) for NN weight storage, along with an inertial measurement unit (IMU) (LSM6DSO, ST Microelectronics) for device interaction and motion sensing, and a Power Management Integrated Circuit (PMIC) (MAX20303, Analog Devices) for efficient power regulation.

2) *Bio-potential expansion board*: stacked on top of the baseboard, it extends the system's capabilities with a biopotential measurement AFE (ADS1298, Texas Instruments). The design supports EEG data acquisition of 8 channels at a 24-bit resolution. Unless otherwise stated, we operate the ADS1298 at a sampling rate of 1 kSPS and a gain of 6 in high-resolution mode. The system is characterized by an integrated root mean square (RMS) noise of  $0.47 \mu\text{V}$  in the frequency range of 0.5 to 100 Hz, which aligns with the standards set by the International Federation of Clinical Neurophysiology (IFCN) for recording EEG signals in clinical settings [28]. Additionally, the board incorporates a subsystem dedicated to evaluating electrode contact quality, ensuring the reliability and clarity of the EEG signals collected [29].

3) *Channel-selection interface PCB*: with BioGAP capable of processing up to 8 channels concurrently, this PCB (shown in Fig. 1, D) selects which subset of channels (out of the 8 EEG + 3 EOG channels available in the frame) to use for concurrent measurement. Two distinct channel-selection PCBs are designed to explore two configurations:

- The *EEG-only* configuration allows concurrent measurement of the six temple electrodes and two BTE electrodes.
- The *combined EEG-EOG* configuration selects two EEG electrodes per side as well as the three EOG electrodes on the nose bridge and pads that allow for the measurement of the vertical and horizontal EOG.

The BioGAP electronics, along with a 75 mAh rechargeable battery, are integrated into a compact, 3D-printed enclosure, measuring  $40 \times 30 \times 15 \text{ mm}^3$ . The box can be discretely attached to the back of the head and is connected through the flexible channel-selection interface PCB to the electronics inside the glasses frame.

#### F. System integration

The integrated platform is assembled by inserting the EEG electrodes into the PTH of the electrode interface PCB, where each electrode is paired with an opamp for active signal buffering. The EOG electrodes are plugged into a hollow metal rod embedded in the frame, connected via wires to the active buffering stages. The electrodes interface PCB is fully embedded within the frame and connects to the BioGAP platform through the channel-selection PCB that allows configuration changes between the EEG only and the combined EEG-EOG configuration. Then, the frame is closed with lids that are secured with screws. Finally, the BioGAP box (containing

BioGAP, battery, power switch, and giving access to a micro USB charging connector) can be secured on a band behind the head, which also ensures the proper fit of the glasses. The fully assembled prototype weights 40 g and has a size of  $160 \times 145 \text{ mm}^2$

## IV. VALIDATION

This section presents experimental results to verify the design of the prototype. These results serve as a validation step to demonstrate that GAPSES can acquire high-quality ExG data.

Here, BioGAP is operated at a sampling frequency of 500 Hz and with a programmable-gain amplifier (PGA) of 12. All the experimental procedures followed the principles outlined in the Helsinki Declaration of 1975, revised in 2000.

### A. Validation of EOG subsystem

To showcase the feasibility of measuring EOG with the given electrode configuration, a subject was instructed to wear the glasses and execute a series of saccadic eye movements: up, down, right, left, up-right, up-left, down-right, down-left, blink, and double-blink. The glasses were used with the combined EEG-EOG channel-selection interface PCB, as described in section III-E, giving access to all three EOG channels. Visual inspection of the EOG signals allows to verify the validity of the measurements.

The vertical ( $V_V$ ) and horizontal ( $V_H$ ) EOG signals are computed according to equations (1–2):

$$V_V = V_C - \frac{(V_R + V_L)}{2} \quad (1)$$

$$V_H = V_R - V_L \quad (2)$$

where  $V_R$ ,  $V_L$ , and  $V_C$  are the signals measured from the EOG electrodes on the right side of the nose, on the left side of the nose, and the center of the glass bridge, respectively.

The offset and signal drift are removed by subtracting the running mean with a window size of 2 s and the signal is subsequently smoothed with a 10-th order IIR Butterworth low-pass filter with a 40 Hz cutoff frequency. Figure 2 shows a series of eye movements, where the subject is instructed to look from the center to the respective direction (e.g., to the right, left, etc.) and then right back to the center. Purely vertical eye movements (up, down) show a strong response of the vertical EOG in the respective direction, while the horizontal EOG amplitude stays low. Conversely, purely horizontal eye movements (right, left) show a strong response in the horizontal EOG component, while the vertical signal remains low. Diagonal eye movements (up-right, up-left, down-right, and down-left) result in the respective combination of horizontal and vertical EOG signal. Finally, blink and double-blink result in one and two short peaks in the vertical EOG signal. The distinct signal shape of each eye movement confirms the feasibility of acquiring high-quality EOG signals with the given electrode positions and distinguishing between the chosen eye movements, while the fast sequence of distinct movements suggests the feasibility of implementing a HMI with a high ITR (Sect. V provides more insights into EOG-based applications).

### B. Validation of EEG subsystem

1) *Alpha waves*: A subject was tested in an alpha waves experiment using the glasses in the EEG-only configuration. The subject was instructed to alternate between closed and open eyes states for 30 seconds each, as this paradigm is commonly used as a qualitative marker for EEG-based systems in both medical and HMI applications

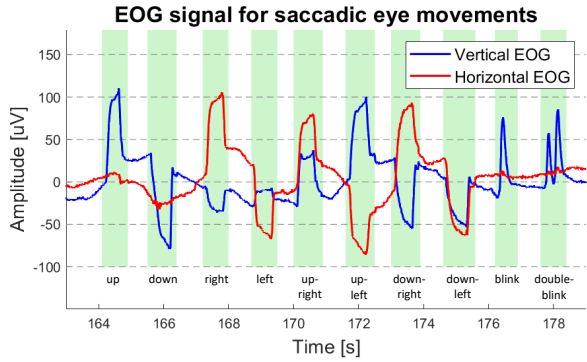


Fig. 2. Measurement of the horizontal and vertical EOG signal while different eye movements are performed.

[30]. Figure 3 shows the signal spectrogram (1024 samples=2.048 s windows with a 768 samples=1.536 s overlap) of the channel 4 in the EEG configuration (CFR. Fig. 1, D). As expected, a strong increase in the energy component for the alpha band is evident when the subject was instructed to close the eyes.

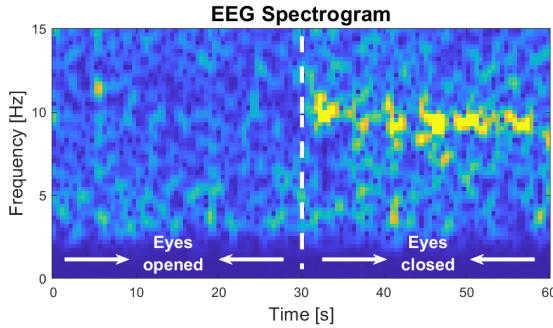


Fig. 3. Spectrogram of the EEG system evaluation by performing alpha waves measurement in the eyes open vs eyes closed experiment.

2) *SSVEP*: SSVEP is a frequency-and-phase-locked EEG response to repetitive visual stimuli [31], frequently employed as a control paradigm in SoA BCIs. We evaluated the glass’s performance for five subjects. Subjects were sitting in front of a 14-inch computer screen at approximately 60 cm distance. Stimuli, consisting of sinusoidal on-off patterns with 100% contrast, were presented sequentially on the screen. Pattern’s frequency include 7.5 Hz, 11.5 Hz, 13.5 Hz, and 15.5 Hz, and were presented in a random order, across three repetitions. Each frequency was presented for 25 seconds, followed by a 10-second rest period to mitigate visual fatigue. EEG response is measured through the Normalized Canonical Correlation Analysis (NCCA) [32]. NCCA extends the canonical-correlation analysis (CCA) by focusing on the detection of a specific “peak” frequency within EEG data. NCCA hence, provides the ratio of the CCA response at a target frequency to the average response at two adjacent frequencies. In this work,  $NCCA^1$  is computed on data segments from each trial, with results averaged among all available trials. The results for each target frequency (colored continuous lines) are presented in Fig 4 (A), with increasingly larger CCA evaluation windows. NCCA is also computed for rest trials (grey dashed lines) to provide evidence of the correct operation of the NCCA index algorithm. For all frequencies, a window of 3 s is sufficient to identify

<sup>1</sup>Side frequencies for NCCA calculation are always  $\pm 0.2$  Hz from the target frequency.

SSVEP response with sufficient confidence<sup>2</sup>. For reference, Fig 4 (B) also presents the frequency response (based on the CCA algorithm) for all four frequencies for subject 1, each denoting clear power peaks that are always above power values of neighbor frequencies and the rest segments.

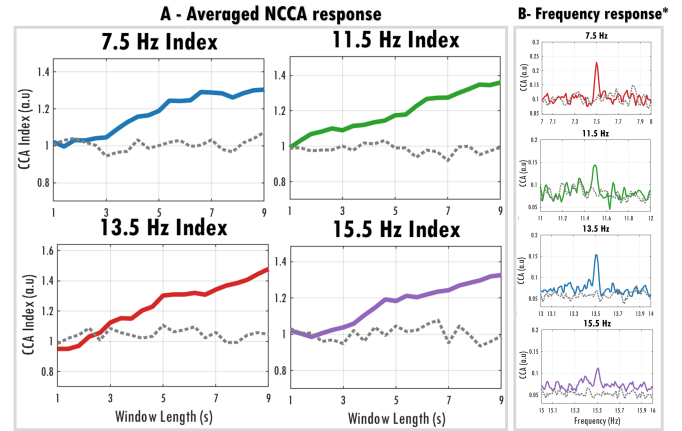


Fig. 4. (A) NCCA of the SSVEP experiment showing the response at different window lengths (average values across five subjects). (B) corresponding CCA for one subject.

3) *MM*: The glasses were further validated on a MM protocol, in light of its popularity among BCI paradigms and to verify signals originated from the motor cortex. Five subjects performed right and left-hand movements (finger tapping [33]) interleaved by rest periods while EEG data were recorded. Trial duration (gesture+rest) is, on average, 10s, with gestures lasting 4s and rests of random duration between 5 and 6 seconds. Subjects followed visual instructions on a screen placed ca. 1m away, and each instruction synchronized with the EEG data through a digital triggering system on BioGAP. MMclassification performance is assessed through MI-BMInet [34], a lightweight, embedded convolutional neural network (CNN) that demonstrated SoA classification accuracy for this task. The accuracy obtained through the classifications is reported on the basis of a rolling window Cross Validation (CV) on a validation set. We train the models (subject-specific) for 500 epochs using cross-entropy loss, Adam optimizer (lr=0.001), and a batch size of 64.

Before training and inference, EEG data are preprocessed with a notch filter at 50 Hz and a 4<sup>th</sup> order IIR band-pass filter at 0.5–100 Hz and downsampled by a factor of 2, obtaining 950 samples in time. Table I presents the 2-class (left vs. right) and 3-class (left vs. right vs. rest) classification results of MI-BMInet for all five subjects and the resulting average. Peak classification performance is achieved by S1, with 67% and 49% of accuracy for the 2-class and 3-class classification, respectively. The reported averaged values are also above chance (11.2% and 8.92% for 2-class and 3-class, respectively), indicating the device’s ability to retrieve basic MM events.

## V. EOG APPLICATION: AUTOMATED SACCADIC EYE MOVEMENT CLASSIFICATION

Sect. IV validated the acquisition of EOG signals with GAPSES based on visual inspection. In this section, we automate the eye movement classification task by deploying on the device an energy-efficient classification pipeline, demonstrating a competitive ITR performance

<sup>2</sup>Empirical data show that NCCA values above 1.1 significantly correlate to the presence of EEG SSVEP response.

TABLE I  
ACCURACY SCORES FOR THE MM CLASSIFICATION TASK.

Subject	2 class accuracy [%]	3 class accuracy [%]
S0	57	37.33
S1	67	49.33
S2	59	41.33
S3	62	40
S4	61	43.33
<b>Average</b>	<b>61.2</b>	<b>42.26</b>

at ultra-low power. These results demonstrate that GAPSES are well-suited for wearable and fast Human-Machine interactions, e.g. for assisted spelling or gaming.

#### A. Data acquisition protocol

Five subjects participated in an eye movement experiment where the horizontal and vertical EOG was measured while the subjects were seated in a stationary position. A Python script (based on Psychopy) provided the subject with visual instructions on a monitor on which eye movement should be performed. The measured raw data were streamed to a Java GUI and saved alongside the ground truth labels provided by the Psychopy script. The subjects performed the eye movements freely, with no specific fixation point to guide them. While this might lead to a slight decrease in accuracy, it is expected to result in a more diverse dataset that improves the robustness of the model in realistic scenarios and less constrained settings. The dataset encompasses 11 classes (up, down, right, left, up-right, up-left, down-right, down-left, blink, double-blink, rest), with two sessions per subject and removal/repositioning of the glasses between sessions (to introduce inter-session variability mimicking realistic use-case scenarios, where end users do not wear the device all the time). Each session involved recording 25 trials, each with a duration of 2 s, for every class of eye movement, resulting in 50 samples per class for each subject.

#### B. Data processing pipeline and classification model

Firstly, we calculate the vertical and horizontal EOG signals using equations 1 and 2, respectively. Then, we apply a bandpass filter between 0.5 and 40Hz and apply a moving average filter on the signal. The moving average filter uses a window size of 2 seconds and only takes into account past data for averaging removal. We segment the measured data stream into samples corresponding to individual eye movements using the time-synchronized ground-truth labels. The classification task is based on a modified version of the EPIDeNET network [35], adapted to classify EOG signals. The modified network, detailed in Table II, includes a parameterization of the kernel size for the last MaxPool layer to be either 1 for EOG signals or 4 for EEG signals.

#### C. Results

We evaluated our approach via a 5-fold cross-validation. We examined both a 'global' model, which was trained on all subjects, and a subject-specific model. The average accuracy of the global model was 94.91% (not shown), while the subject-specific model achieved an average accuracy of 96.78%. Fig. 5 (blue curve) shows how the subject-specific accuracy changes when only a fraction of the 2-second windows is considered. The maximum accuracy is achieved when the entire 2-second window is used.

Additionally, we visualized the features the EPIDeNET model outputs from the last convolutional layer using t-SNE [37]. The

TABLE II  
EPIDeNET ARCHITECTURE [36]

Type	#Filters	Kernel	Output	
$\phi^1$	Conv2D	4	(1, 4)	(4, C, T)
	MaxPool	(1, 8)	(4, C, T // 8)	
$\phi^2$	Conv2D	16	(1, 16)	(16, C, T // 8)
	MaxPool	(1, 4)	(16, C, T // 32)	
$\phi^3$	Conv2D	16	(1, 8)	(16, C, T // 32)
	MaxPool	(1, 4)	(16, C, T // 128)	
$\phi^4$	Conv2D	16	(16, 1)	(16, C, T // 128)
	MaxPool	(D, 1)	(16, C // 4, T // 128)	
$\phi^5$	Conv2D	16	(8, 1)	(16, C // 4, T // 128)
	AdaptiveAveragePool		(16, 1, 1)	
$\phi^6$	Dense		2	

$C$  = number of channels,  $T$  = number of time samples,  $D = 1$  for EOG data and  $D = 4$  for EEG data

inset in Fig. 5 shows the 2-dimensional representation of the feature space explored by EPIDeNET. Similar movements (such as double blinks and single blinks) are grouped together, and most errors in the subsequent classification derive from the selected boundary between these classes.

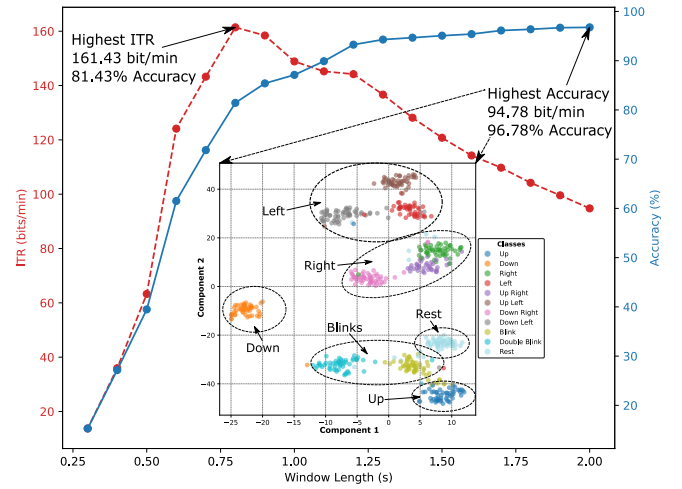


Fig. 5. Averaged Accuracy and ITR values for the subject-specific models when considering different fractions of the 2-second windows. Inset: t-SNE visualization of the highest accuracy point.

The ITR is computed based on equation 3:

$$ITR = \frac{60(\log_2 M + P \log_2 P + (1 - P) \log_2 \frac{1-P}{M-1})}{T} \quad (3)$$

with  $T$  being the window length,  $P$  being the accuracy of the classification, and  $M$  being the number of different tasks (11 in our case). Fig. 5 (red line) shows how the ITR changes with the considered window length. The maximum ITR is achieved for  $T = 0.8$  s, with a corresponding performance (accuracy) of  $P = 0.814$ , and is equal to  $ITR_{\max} = 161$  bit/min.

#### D. Embedded implementation

We deploy our model on the GAP9 platform. We employ Quantlab [38] to convert neural networks into the INT-8 format (a step needed for adapting the models to low-power embedded platforms). Additionally, the deployment process is facilitated by DORY [39], a specialized tool that autonomously generates C code tailored for managing the two-tier memory architecture—L1 and L2 memory—found in PULP-based systems. DORY optimizes memory utilization, ensuring that our deployment maximizes efficiency and effectiveness in resource-limited environments. Table IV (EOG columns) shows the result of the embedded implementation when considering two

alternative input sizes (either 500 or 1000 samples, for the two EOG signals  $V_H$  and  $V_V$ ), achieving a peak energy efficiency of 12.24 GMAC/s/W, an energy per inference as low as 0.024 mJ, and an average power consumption of only 16.02 mW.

### E. Comparison to SoA for EOG-based eye movement classification

GAPSES achieve competitive performance in eye movement classification (peak of 96.78%), also when compared to conventional acquisition setups. In fact, [40] demonstrated an accuracy of 88.59% for eight distinct eye movements and single blinks, and [41] achieved an accuracy of 96.9% for six saccades classes coupled with a 97.33% eye-blink detection accuracy. Considering alternative wearable devices, [42] used the JINS MEME smart glasses to develop an EOG speller and classified 16 distinct eye movements and a rest class using a thresholding algorithm, resulting in a classification accuracy that is significantly lower (73.78%) than the accuracy achieved in this work.

The achieved ITR also proved to be competitive. Compared to the recent work of [43], which achieved an ITR of 38 bit/min with a single-channel EOG, GAPSES offers an approx.  $4\times$  higher performance. Additionally, our ITR also surpasses the 108.63 bits/min achieved by [44] with a hybrid EOG-SSVEP approach.

These results demonstrate that GAPSES coupled with EPIDENET is a leading-edge solution for low-power and fast EOG-based HMIs.

## VI. EEG APPLICATION: BRAINMETRICS

Sect. IV validated the acquisition of EEG signals with GAPSES based on the most common paradigms (alpha waves, SSVEP, MM). In this section, we demonstrate the application of GAPSES for EEG-based biometrics (BrainMetrics), i.e., to identify the glasses' owner through their unique brainwave patterns. This feature allows for a more personalized and secure interaction with the device. By verifying the user's identity with EEG-based biometrics, BrainMetrics ensures that only the authorized user can access the device's advanced features, such as the EOG-based interaction (previous section).

### A. Data acquisition protocol

Six healthy subjects participated in three separate sessions spread over multiple days, ensuring a diverse dataset with multiple repositioning of the glasses. During each session, we conducted half an hour of EEG data acquisition with the EEG-only configuration of the glasses (see Fig. 1, D) that allows concurrent measurement of eight EEG channels along the temples and BTE. To capture a diverse set of data reflective of typical daily activities, subjects could engage in their normal routines, such as working on a computer, reading, and watching television. However, to mitigate the impact of motion artifacts on the data quality, we requested that all participants remain seated throughout the experiment. Additionally, subjects were advised to minimize talking to reduce further potential disruptions in the EEG recordings.

### B. Data processing pipeline and model architecture

Data are first band-pass filtered within the 0.5 Hz to 100 Hz range, and subsequently, we apply a 50 Hz notch filter to remove any electrical noise. A moving average filter with a duration of 0.5 seconds is utilized to enhance the uniformity of the data. The segmented data are organized into 4-second intervals, each assigned a label from 0 to 5, indicating the specific subject the data originated from. Regarding the model architecture, we employ EPIDENET [35] in light of its robustness and energy-efficient performance, particularly on the GAP9 platform.

TABLE III  
BRAINMETRICS ACCURACY, SENSITIVITY AND, SPECIFICITY SCORES FOR SUBJECT-SPECIFIC MODELS.

Metric	Subject	Mean (8 channels)	Mean (4 Channels)
Accuracy	S0	99.91 $\pm$ 0.04	99.93 $\pm$ 0.05
Accuracy	S1	99.57 $\pm$ 0.15	99.57 $\pm$ 0.15
Accuracy	S2	99.89 $\pm$ 0.04	99.89 $\pm$ 0.04
Accuracy	S3	99.84 $\pm$ 0.14	99.84 $\pm$ 0.14
Accuracy	S4	99.32 $\pm$ 0.16	99.30 $\pm$ 0.12
Accuracy	S5	99.92 $\pm$ 0.07	99.91 $\pm$ 0.10
Accuracy	mean	99.74 $\pm$ 0.11	99.74 $\pm$ 0.11
Sensitivity	S0	99.74 $\pm$ 0.19	99.79 $\pm$ 0.22
Sensitivity	S1	99.80 $\pm$ 0.20	99.80 $\pm$ 0.21
Sensitivity	S2	99.36 $\pm$ 0.25	99.27 $\pm$ 0.24
Sensitivity	S3	98.07 $\pm$ 1.83	98.07 $\pm$ 1.83
Sensitivity	S4	96.76 $\pm$ 0.96	96.51 $\pm$ 0.96
Sensitivity	S5	99.49 $\pm$ 0.29	99.49 $\pm$ 0.29
Sensitivity	mean	98.87 $\pm$ 0.87	98.82 $\pm$ 0.87
Specificity	S0	99.96 $\pm$ 0.05	99.98 $\pm$ 0.04
Specificity	S1	99.48 $\pm$ 0.14	99.48 $\pm$ 0.14
Specificity	S2	99.98 $\pm$ 0.04	100.00 $\pm$ 0.00
Specificity	S3	99.97 $\pm$ 0.04	99.97 $\pm$ 0.04
Specificity	S4	99.79 $\pm$ 0.09	99.81 $\pm$ 0.11
Specificity	S5	99.97 $\pm$ 0.07	99.95 $\pm$ 0.10
Specificity	mean	99.86 $\pm$ 0.08	99.87 $\pm$ 0.09

### C. Results

We explore a subject-specific model approach, i.e., we train a dedicated model for each subject, specialized in identifying whether the EEG signature belongs to the particular subject it's trained on. Hence, the model operates in a 2-class modality, classifying "owner" vs "non-owner" of the glasses. We segment the data and employ a 5-fold cross-validation technique to obtain a reliable assessment of the model's precision. Additionally, we evaluate the outcomes when employing all eight electrodes versus using just four electrodes for the classification task. This comparison demonstrates the methodology's robustness in maintaining high accuracy levels, even when only a partial set of channels is utilized.

Table III shows the classification results and reveals a high average specificity (99.86), coupled with a high sensitivity (98.87). These findings indicate that a subject-specific model constitutes an effective strategy for BrainMetrics applications.

### D. Embedded implementation

We use the same deployment procedure presented in Sect. V-D for the EOG embedded implementation. Table IV (EEG column) shows the achieved performance for the deployment of BRAINMETRICS on GAPSES. We demonstrate an energy efficiency as high as 31.64 GMAC/s/W, coupled with an energy per inference of only 0.121 mJ and average power consumption as low as 26.54 mW.

### E. Comparison to SoA for EEG-based biometrics

A large number of subjects is commonly employed for assessing EEG-based biometrics (typically greater than 20). Our analyses are based on fewer subjects (6) as a feasibility study of BrainMetrics with GAPSES. Since most of the related works report accuracy metrics, we base the following comparison on the mean accuracy achieved by GAPSES, i.e., 99.74% (for eight channels).

Our accuracy is comparable to that achieved with EEG-cap setups by [45] (98.97% accuracy, based on a motor-imagery paradigm) and [46] (99.86% validation accuracy, based on a multi-task approach). Additionally, our classification accuracy also surpasses the performance of works employing a similar number of subjects and

TABLE IV

IMPLEMENTATION OF THE EOG AND BRAINMETRICS NETWORK ON GAP9

Network Data	EPIDeNET*	EPIDeNET*	EPIDeNET*
	EOG		EEG
Platform (MCU)	GAP9 (1+9×RISCY @240 MHz)		
Deployment framework	Quantlab/DORY		
Input size	2 × 500	2 × 1000	8 × 2000
MACs	259,856	484,752	3,844,000
Time/inference [ms]	<b>1.50</b>	<b>2.47</b>	<b>4.58</b>
Throughput [MMAC/s]	<b>173.47</b>	<b>196.10</b>	<b>839.67</b>
MACs/cycle	<b>0.72</b>	<b>0.82</b>	<b>3.50</b>
Power [mW]	<b>16.28</b>	<b>16.02</b>	<b>26.54</b>
Energy/inference [mJ]	<b>0.024</b>	<b>0.040</b>	<b>0.121</b>
En. eff. [GMAC/s/W]	<b>10.66</b>	<b>12.24</b>	<b>31.64</b>

channels ([47], presenting an accuracy of 97.6% based on five users, 8 channels, and combined Visual-evoked potentials and Event-related potential protocol).

These results demonstrate the EEG functionality of GAPSES, which can be potentially used as a biometric tool to 'unlock' the fast EOG functionalities only to the identified user.

## VII. COMPARISON TO STATE-OF-THE-ART EXG-BASED SMART GLASSES

Table V summarizes the positioning of GAPSES in the context of existing smart glasses for EEG and EOG acquisition. GAPSES stands out with a notably higher channel count, featuring 8 EEG and 3 EOG channels, while existing solutions are either restricted to a single modality or a single channel per modality. In terms of power consumption, the total system power consumption of GAPSES when streaming raw data is significantly lower compared to related works (30 mW compared to 111 mW in [17] and 300 mW [18]). Additionally, to the best of our knowledge, GAPSES is the only device offering substantial edge processing capabilities, enabling computations at the edge with high energy efficiency.

## VIII. CONCLUSION

In this paper, we presented GAPSES, a smart-glasses platform for fully dry and wearable EEG and EOG measurement. We described the system design, which involved the development of custom ExG electrodes based on soft conductive rubber (to ensure comfort and good signal quality for extended wearing durations), custom mechanical frames, and electronics interfaces to a PULP ExG acquisition and processing platform.

We first validated GAPSES' functionality across various common tasks such as alpha wave detection, SSVEP, and MM classification. Additionally, we showcased the device's potential in two end-user applications. Using the device as an EOG-based HMI end-to-end, we demonstrated an accuracy as high as 96.78% in an eye-movement classification task that discriminates among 11 classes, also demonstrating an ITR as high as 161.43 bit/min. Using the device as an EEG-based BrainMetrics solution, we demonstrated a subject-specific identification task with average sensitivity and specificity as high as 98.87% and 99.86%, respectively. These two applications are deployed on the device and consume only 24 μJ and 121 μJ per inference (for the EOG and EEG application, respectively), operating at a total power of only 16.28 mW and 26.54 mW (for the EOG and EEG application, respectively). Considering the use-case of BrainMetrics to unlock the device for the owner, followed by a long-term utilization of the EOG features, the sub-20 mW power consumption enables continuous acquisition and online processing of EOG signals for more than 12 h with a small 75 mAh battery.

Overall, GAPSES sets a new SoA by offering multi-channel acquisition and energy-efficient onboard processing of EEG and EOG signals in a compact, user-friendly glasses form factor, thus addressing many of the limitations found in previous designs. Future research will focus on leveraging these advancements in unconstrained study settings to expand the device's applications.

## ACKNOWLEDGMENT

We thank L. Mei, A. Blanco Fontao, and H. Gisler (ETH Zürich) for technical support.

## REFERENCES

- [1] D. Dias and J. Paulo Silva Cunha, "Wearable health devices—vital sign monitoring, systems and technologies," *Sensors*, vol. 18, no. 8, p. 2414, Jul. 2018.
- [2] T. Yilmaz, R. Foster, and Y. Hao, "Detecting vital signs with wearable wireless sensors," *Sensors*, vol. 10, no. 12, p. 10837–10862, Dec. 2010.
- [3] I. Hussain and S. J. Park, "Healthsos: Real-time health monitoring system for stroke prognostics," *IEEE Access*, vol. 8, pp. 213 574–213 586, 2020.
- [4] OpenBCI, <http://openbci.com/>, 2018, Accessed: 24-05-2024.
- [5] Emotiv, <https://www.emotiv.com/>, 2018, Accessed: 24-05-2024.
- [6] A. J. Casson, "Wearable eeg and beyond," *Biomedical Engineering Letters*, vol. 9, no. 1, p. 53–71, Jan. 2019.
- [7] E. Park, "User acceptance of smart wearable devices: An expectation-confirmation model approach," *Telematics and Informatics*, vol. 47, p. 101318, 2020.
- [8] S. Verwulgen *et al.*, "Determining comfortable pressure ranges for wearable eeg headsets," in *Advances in Human Factors in Wearable Technologies and Game Design*. Cham: Springer International Publishing, 2019, pp. 11–19.
- [9] A. J. Casson, D. C. Yates, S. J. Smith, J. S. Duncan, and E. Rodriguez-Villegas, "Wearable electroencephalography," *IEEE Engineering in Medicine and Biology Magazine*, vol. 29, no. 3, pp. 44–56, 2010.
- [10] V. V. Tipparaju, K. R. Mallires, D. Wang, F. Tsow, and X. Xian, "Mitigation of data packet loss in bluetooth low energy-based wearable healthcare ecosystem," *Biosensors*, vol. 11, no. 10, p. 350, Sep. 2021.
- [11] Neurosky, "Neurosky MindWave," <http://neurosky.com/biosensors/eeg-sensor/biosensors/>, 2018, Accessed: 24-05-2024.
- [12] F. Tian *et al.*, "The three-lead eeg sensor: Introducing an eeg-assisted depression diagnosis system based on ant lion optimization," *IEEE Transactions on Biomedical Circuits and Systems*, vol. 17, no. 6, pp. 1305–1318, 2023.
- [13] J. H. Shin *et al.*, "Wearable eeg electronics for a brain-ai closed-loop system to enhance autonomous machine decision-making," *npj Flexible Electronics*, vol. 6, no. 1, May 2022.
- [14] Nordic Semiconductor, "Bluetooth low energy data throughput," <https://infocenter.nordicsemi.com>, Accessed: 10-03-2023.
- [15] S. Frey *et al.*, "BioGAP: a 10-core FP-capable ultra-low power IoT processor, with medical-grade AFE and BLE connectivity for wearable biosignal processing," in *2023 IEEE International Conference on Omni-layer Intelligent Systems (COINS)*, 2023, pp. 1–7.
- [16] D. Sopic, A. Aminifar, and D. Atienza, "e-Glass: A Wearable System for Real-Time Detection of Epileptic Seizures," in *2018 IEEE International Symposium on Circuits and Systems (ISCAS)*, 2018, pp. 1–5.
- [17] N. Kosmyna, C. Morris, U. Sarawgi, T. Nguyen, and P. Maes, "AttentivU: A wearable pair of eeg and eog glasses for real-time physiological processing," in *2019 IEEE 16th International Conference on Wearable and Implantable Body Sensor Networks (BSN)*. IEEE, May 2019.
- [18] J. H. Lee *et al.*, "3D printed, customizable, and multifunctional smart electronic eyeglasses for wearable healthcare systems and human-machine interfaces," *ACS Applied Materials & Interfaces*, vol. 12, no. 19, p. 21424–21432, Apr. 2020.
- [19] "Smith lowdown focus eyewear glasses," <https://solsticesunglasses.com/pages/smithlowdownfocus>, Solstice Sunglasses, [Accessed 24-05-2024].
- [20] "Jins meme," <https://jinsmeme.com/>, [Accessed 24-05-2024].
- [21] "Imec glasses," <https://www.imec-int.com/en/imec-magazine/imec-magazine-september-2018/glasses-that-keep-an-eye-on-your-health>, [Accessed 24-05-2024].
- [22] "Datwyler SoftPulseTM," <https://datwyler.com/softpulse>, [Accessed 24-05-2024].

TABLE V  
COMPARISON TO SOA SMART GLASSES FOR EEG AND EOG ACQUISITION.

Device	# of biopotential channels (Application)	Electrodes	Power consumption [mW]	SoC	Performance [Mop/s]	Energy efficiency [Mop/s/mW]
AttentiveU [17]	1 EEG (AW) 1 EOG (visual inspection)	Silver	111 (stream)	12 MHz MCU	N/A	N/A
[18]	1 EEG (AW, SSVEP) 1 EOG (visual inspection, eye movement classification)	Carbon nanotube/polydimethylsiloxane composite	300 (stream)	ATmega128	16 (int8)	0.24 (int8)
e-Glass [16]	4 EEG (SD <sup>1</sup> )	N/A	32.4 (online SD <sup>1</sup> )	STM32L151	32 (int32)	2.35 (int32)
<b>GAPSES (this work)</b>	<b>8 EEG (AW, SSVEP, MM, Brainmetrics)</b> <b>3 EOG (visual inspection, eye movement classification)<sup>2</sup></b>	<b>Soft conductive rubber with Ag/AgCl coating</b>	<b>30 (stream)</b> <b>16.28 (online eye movement classification)</b>	<b>GAP9</b>	<b>3'000 (FP32)</b>	<b>74 (FP32)</b>

AW: Alpha Waves, SSVEP: Steady-State Visual Evoked Potential, MM: Motor Movement classification, SD: Seizure Detection, FP: floating point  
(1) results based on online dataset, (2) concurrent acquisition of up to 8 channels

- [23] Y.-H. Chen *et al.*, "Soft, comfortable polymer dry electrodes for high quality eeg and eeg recording," *Sensors*, vol. 14, no. 12, p. 23758–23780, Dec. 2014.
- [24] M. Guermandi, A. Cossetini, S. Benatti, and L. Benini, "A wireless system for eeg acquisition and processing in an earbud form factor with 600 hours battery lifetime," in *Annu. Int. Conf. IEEE Eng. Med. Biol. Soc.*, vol. 2022, 2022, pp. 3139–3145.
- [25] "ISO 10993-5," Bureau for Standardization (NBN), Schattdorf, Switzerland, 2009.
- [26] "ISO 10993-10:2021," International Organization for Standardization, Geneva, Switzerland, 2021, available from: ANSI Webstore.
- [27] ML Commons, "MLPerf Inference: Tiny Benchmark Suite Results, v1.0," 2022, Accessed: 24-05-2024. [Online]. Available: <https://mlcommons.org/benchmarks/inference-tiny/>
- [28] M. R. Nuwer *et al.*, "IFCN standards for digital recording of clinical EEG," *Electroencephalography and clinical Neurophysiology*, vol. 106, no. 3, pp. 259–261, 1998.
- [29] V. Kartsch, S. Benatti, D. Rossi, and L. Benini, "A wearable eeg-based drowsiness detection system with blink duration and alpha waves analysis," in *2017 8th International IEEE/EMBS Conference on Neural Engineering (NER)*, 2017, pp. 251–254.
- [30] Ö. Türk and M. S. Özerdem, "Determination of changes in frequencies of eeg signal in eyes open / closed duration," in *2015 23rd Signal Processing and Communications Applications Conference (SIU)*. IEEE, 2015, pp. 2617–2617.
- [31] D. Zhu, J. Bieger, G. Garcia Molina, and R. M. Aarts, "A survey of stimulation methods used in ssvp-based bcis," *Computational intelligence and neuroscience*, vol. 2010, 2010.
- [32] V. J. Kartsch *et al.*, "Efficient low-frequency ssvp detection with wearable eeg using normalized canonical correlation analysis," *Sensors*, vol. 22, no. 24, p. 9803, 2022.
- [33] H. Cho, M. Ahn, M. Kwon, and S. Jun, "A step-by-step tutorial for a motor imagery-based BCI," in *Brain-Computer Interfaces Handbook: Technological and Theoretical Advances*, F. L. Chang S. Nam, Anton Nijholt, Ed. Taylor & Francis Group, 2018, ch. 23, pp. 445–460.
- [34] X. Wang, L. Mei, V. Kartsch, A. Cossetini, and L. Benini, "Enhancing performance, calibration time and efficiency in brain-machine interfaces through transfer learning and wearable eeg technology," in *2023 IEEE Biomedical Circuits and Systems Conference (BioCAS)*, 2023, pp. 1–5.
- [35] T. M. Ingolfsson *et al.*, "EpiDeNet: An energy-efficient approach to seizure detection for embedded systems," in *2023 IEEE Biomedical Circuits and Systems Conference (BioCAS)*, 2023, pp. 1–5.
- [36] —, "Towards Long-term Non-invasive Monitoring for Epilepsy via Wearable EEG Devices," in *2021 IEEE Biomedical Circuits and Systems Conference (BioCAS)*, 2021, pp. 01–04.
- [37] L. Van der Maaten and G. Hinton, "Visualizing data using t-sne." *Journal of machine learning research*, vol. 9, no. 11, 2008.
- [38] M. Spallanzani *et al.*, "QuantLab: a Modular Framework for Training and Deploying Mixed-Precision NNs," <https://cms.tinymml.org/wp-content/uploads/talks2022/Spallanzani-Matteo-Hardware.pdf>, March 2022.
- [39] A. Burrello *et al.*, "DORY: Automatic end-to-end deployment of real-world dnns on low-cost iot mcus," *IEEE Transactions on Computers*, vol. 70, no. 8, pp. 1253–1268, 2021.
- [40] S.-L. Wu *et al.*, "Controlling a human-computer interface system with a novel classification method that uses electrooculography signals," *IEEE Transactions on Biomedical Engineering*, vol. 60, no. 8, p. 2133–2141, Aug. 2013.
- [41] B. O'Bard and K. George, "Classification of eye gestures using machine learning for use in embedded switch controller," in *2018 IEEE International Instrumentation and Measurement Technology Conference (I2MTC)*. IEEE, May 2018.
- [42] N. Barbara and T. A. Camilleri, "Interfacing with a speller using eeg glasses," in *2016 IEEE International Conference on Systems, Man, and Cybernetics (SMC)*, Oct. 2016.
- [43] S. He and Y. Li, "A single-channel eeg-based speller," *IEEE Transactions on Neural Systems and Rehabilitation Engineering*, vol. 25, no. 11, pp. 1978–1987, 2017.
- [44] J. Zhang, S. Gao, K. Zhou, Y. Cheng, and S. Mao, "An online hybrid bci combining ssvp and eeg-based eye movements," *Frontiers in Human Neuroscience*, vol. 17, p. 1103935, 2023.
- [45] S. Bak and J. Jeong, "User biometric identification methodology via eeg-based motor imagery signals," *IEEE Access*, 2023.
- [46] H. Vadher *et al.*, "Eeg-based biometric authentication system using convolutional neural network for military applications," *Security and Privacy*, vol. 7, no. 2, p. e345, 2024.
- [47] H. Touyama, "Eeg-based personal identification," *Biomedical Engineering, InTech Journal on*, vol. 22, pp. 415–424, 2009.